Defect production in Bi and dilute alloys irradiated by electrons

F. Beuneu and P. Bois
Laboratoire des Solides Irradiés, Ecole Polytechnique, 91128 Palaiseau Cédex, France
(Received 10 August 1987)

Pure bismuth and dilute bismuth alloys (containing tellurium or tin) were electron irradiated at high doses. In most experiments the resistivity was measured during defect production; for some experiments the magnetoresistance and Hall effect were also studied. We analyze the data from this latter experiment type, which enables us to know the variation of the carrier number during irradiation, i.e., the mean charge brought by a defect. The results are in agreement with a simple model which states that the Frenkel pairs are of donor type and are ionized under all circumstances whereas the more complicated defects created at high electronic energy (above 1.2 MeV) are of acceptor type and produce in the density of states a virtual bound state situated slightly below the pure bismuth (intrinsic) Fermi level. These results are in agreement with the conclusions of an earlier paper in which we studied the displacement threshold energy in bismuth. Moreover, our data enable us to state that the recombination volume in bismuth is in the 100–200 atomic volume range.

I. INTRODUCTION

As a semimetal, bismuth is a rather fascinating element, whose physical properties are often very spectacular. Its behavior under irradiation[1] is not an exception in that respect, as the observed effects seem to combine metal and semiconductor-like types of effects. If the physical properties of the semimetal bismuth have been extensively studied in the literature, the doping by point defects, on the other hand, has received much less attention. One can mention the work of Legros–de Mauduit and Reynaud[2] under the electron microscope, or of Weck *et al.*[3] on neutron-irradiated samples. However, a large amount of work has been done in our laboratory on bismuth, concerning quenching,[4] neutron irradiation,[5] and electron irradiation.[1,6,7] Recently, Corbel *et al.*[8] studied positron annihilation in Bi and Bi-based dilute alloys after electron irradiation.

In a preceding paper[9] we presented the results of displacement-threshold-energy measurements performed by electron irradiating bismuth samples (pure or slightly doped with tellurium). We confirmed the published value of Quélard *et al.*:[6] the threshold energy in bismuth is 13 eV. Moreover, our experiment enabled us to draw some conclusions concerning the charge of the irradiation-created defects. These defects were already known to be donors in bismuth.[7] We established in Ref. 9 that the mean defect charge varies with the energy of irradiation: this point is a rather natural consequence of the fact that for a Bi-Te dilute alloy we found the slope and even the sign of the resistivity–versus–electron-dose curves to be energy dependent. More precisely, the mean defect charge decreases from typically 0.2 at low energy to 0.03 at 2.4 MeV. We attributed this fact to the existence of two classes of defects: "simple" one (such as Frenkel pairs) and more "complicated" ones (point-defect complexes, bivacancies, etc.).

We found it interesting to complete these measurements by new experiments, the purpose of which was to get direct insight into the charge of the irradiation defects. In the present paper we describe experiments in which bismuth samples were electron irradiated with a high dose of electrons, the resistivity of the samples being recorded. For some experiments described in this paper, we performed Hall-effect and magnetoresistance measurements during electron irradiation, in order to follow the variation of the number of carriers versus dose. Moreover, in a few cases some Shubnikov–de Haas oscillations were detected. We used not only pure Bi samples, but also dilute alloys of various concentrations. We could thus scan the band structure, varying the Fermi energy according to the concentrations of the acceptor (such as Sn) or donor (such as Te) impurities as established by Noothoven van Goor.[10]

The experimental details are given in Sec. II. In Sec. III we give an account of the experiments in which complete magnetotransport measurements were performed. Also in this section a model is proposed in agreement with our data. Finally, in Sec. IV we describe the higher-dose experiments, where only resistivity was studied, and compare the data with the model of the preceding section. From the highest doses a recombination volume can be extracted.

II. EXPERIMENTAL TECHNIQUES

A. Samples

The samples are cut with a tungsten wire saw from large single crystals obtained from 99.999 95%-pure bismuth, 99.999%-pure tin, and 99.999%-pure tellurium, by melting under vacuum and slow cooling. The quality of our samples, especially concerning possible damage due to the wire saw, is thought to be good, as discussed in Ref. 9. A typical sample is a rectangular slab of area 1×5 mm^2, whose thickness is in the (70–200)-μm range.

We give in Table I the main characteristics of the samples we used. The orientation of the samples, check by x rays, is such that the normal to the slab is the trigonal axis z, whereas the long side is parallel to the binary axis x. The sample Bi I is the only exception, with a normal parallel to the x axis and a long side parallel to the z axis. Five electrical-resistance probes (two for the current, two on one side of the slab for measuring the voltage, and one on the other side for the Hall voltage) made of gold wire are soldered by local melting of the bismuth, so that the electrical current is parallel to the x axis.

We use two methods for determining the Sn or Te concentration of the dilute alloys. The first starts from Hall-effect measurements at 4 K, on the basis of the statement by Noothoven van Goor[10] that tellurium is a monovalent donor and Sn a monovalent acceptor in bismuth. The second is only applicable with good accuracy for tin-doped samples, and relies on another relation found by Noothoven van Goor: the residual-resistivity ratios (RRR's) of Bi-Sn samples vary considerably with Sn content, enabling one to find the tin concentration by measuring the resistivity ratio. The two methods give very similar values.

B. Electron irradiation

The measurements described in the present paper can be classified into two types, which we term hereafter as 4-K experiments and 20-K experiments. The two sets of measurements were performed with our Van de Graaff electron accelerator, the energy of which can be varied from 0.5 to 2.5 MeV. The samples are immersed in the cryogenic coolant and the irradiation is performed through a 25-μm-thick stainless-steel window and a 2-mm-thick liquid-coolant volume: the loss of energy of the electrons before reaching the sample is estimated to 140 keV. The incident electrons are normal to the sample slab, and are thus parallel to the z axis. The dose is determined via the integration of the current measured on a Faraday cage which receives the electron beam behind the sample. The value of 13 eV found in Ref. 9 for the displacement threshold energy enables one to compute the cross sections for a given electron energy and so to know the concentration of defects for a given dose together with their nature: primary defects or complexes.

In the 4-K experiments the samples are immersed in the liquid-helium bath of a classical cryostat. The samples can be put into two positions: in the lower position they are electron irradiated at fluxes such that their temperature remains lower than 10 K. Stopping for a few seconds the irradiation enables one to find resistivity measurements with less noise. From time to time we put—without any heating—the sample holder in the upper position, where magnetoresistance and Hall-effect measurements are performed in a small superconducting coil giving a maximum magnetic field of 1.5 T. All the galvanomagnetic measurements are performed with the field parallel to the trigonal axis z. We used the same four samples throughout the whole 4-K experiment, which included a 1-MeV irradiation with low dose corresponding to 4.5×10^{-5} dpa (displacement per atom) followed by a series of isochronal annealings, a 300-K annealing which proved to give a complete recovery of resistivity and galvanomagnetic parameters, a 2.5-MeV irradiation with doses corresponding to $(2-3)\times10^{-3}$ dpa, and another series of isochronal annealings.

In 20-K experiments the samples are immersed in the liquid-hydrogen bath of a cryostat coupled to a cryogenic machine ensuring a high cooling capacity. The consequence is that higher electron doses could be reached, typically 5 times more than on the 4-K experiments. In the 20-K experiments, however, only the resistance could be measured.

TABLE I. Characteristics of the samples. The sample Bi I has its long side parallel to the z axis.

Sample	Experiment	Thickness (μm)	Initial resistivity ($\mu\Omega$ cm) 4 K	20 K	Dopant content (ppm) From RRR	From Hall
Bi I	20 K	145		12.5		
Bi II	20 K	165		9.8		
Bi III	20 K	80	4.6	10.3		
Bi IV	4 K	83	6.7			0
Bi-Te I	20 K	160	19.7	22.7		71
Bi-Te II	20 K	80	19.4	22.0		75
Bi-Te III	20 K	63		23.8		93
Bi-Te IV	4 K	63	18.1			105
Bi-Sn I	20 K	133		71.1	50	42
Bi-Sn II	4 k	97	114		60	54
Bi-Sn III	20 K	146		108.8	60-80	68
Bi-Sn IV	20 K	80		92.4	90	
Bi-Sn V	20 K	160		75.8	150	139
Bi-Sn VI	4 K	90	52.2		200	213
Bi-Sn VII	20 K	73	43.9	48.7	250	
Bi-Sn VIII	20 K	108	33.9	39.1	400	397

C. Analysis of the 4-K galvanomagnetic measurements

For analyzing the magnetoresistance and Hall-effect data in bismuth, one must remember the complexity of the electronic structure of this semimetal. For a review, see Edel'man.[11] There are two types of carriers in pure bismuth, with an equal concentration of about 3×10^{23} m^{-3}: light electrons and slightly heavier holes. When doped with either Te or Sn, bismuth shifts its Fermi level with, respectively, plus or minus one electronic state per dopant atom.[10] For the present study we used four samples, referenced in Table I, the Fermi levels of which are given in Fig. 1. This figure is a schematic drawing of the band structure of bismuth in the vicinity of the Fermi energy, at the L point of the band structure for the electrons and at the T point for holes. One can see from this figure that there exists a gap at the L point between the electron band and a lower-lying light-hole band with similar effective masses. In the following we make use of Lax's ENP (ellipsoidal nonparabolic) model.[12]

The numerical analysis of the magnetoresistance and Hall-effect curves versus magnetic field is based on the model of Abelès and Meiboom[13] (four independent carrier valleys) improved by Noothoven van Goor.[10] This model gives complex expressions of the Hall coefficient and the magnetoresistivity versus magnetic field for the current taken in the x direction and the field in the z direction; these expressions can be written as

$$\rho_{xx}=\frac{\sigma_{xx}}{\sigma_{xx}^2+\sigma_{yy}^2},$$

$$\rho_{xy}=\frac{\sigma_{xy}}{\sigma_{xx}^2+\sigma_{yy}^2},$$

with

$$\sigma_{xy}(B)=Pe\frac{\nu^2 B}{1+\nu^2B^2}-Ne\frac{\mu_x\mu_y B}{1+\mu_x\mu_y B^2}$$

and

$$\sigma_{xx}(B)=Pe\frac{\nu}{1+\nu^2B^2}+Ne\frac{\frac{1}{2}(\mu_x+\mu_y)}{1+\mu_x\mu_y B^2}.$$

The parameters for this model are the carrier concentrations N (for electrons), P (for holes), P_l (for light holes in the case of Bi-Sn samples where the Fermi level is below the gap at L point; this type of carrier can be formally identified with electrons in the equations, so P_l plays a role equivalent to N), and three mobility parameters, termed here μ_x, μ_y, and ν [μ_x and μ_y are the electron (or light-hole) mobilities in the x and y directions for one electron ellipsoid and ν is the hole mobility], isotropic in the x-y plane. It is wise in practice, to use $\bar{\mu}=\frac{1}{2}(\mu_x+\mu_y)$, $\mu_x\mu_y$, and ν as mobility parameters. In Fig. 2 we give an example of the quality of the fits obtained for the sample Bi-Si II for several doses at 2.5 MeV.

We make a numerical fit of these five parameters (two carrier concentrations, three mobilities) on the whole Hall-effect and magnetoresistance curves, putting, however, 10 times more weight on Hall-effect curves in order to take into account the remark of Noothoven van Goor,[10] who states that magnetoresistance is more sensitive than Hall effect to eventual dopant inhomogeneities. Like Noothoven von Goor, we used the numerical algorithm based on Davidon's method, proposed by Fletcher and Powell,[14] to perform a least-squares fit on our experimental data. We found it very important not to extract the $N-P$ value from the high-field value of the Hall coefficient, because it is in general, far from being saturated at 1.5 T. In some cases the five-parameter fit was greatly undetermined, so we preferred to impose one more relation: that which relates, in the ENP model, N with P. From the Shubnikov–de Haas oscillations detected in the pure Bi sample at 4K (Bi IV), we could verify the validity of this relation; the same was true for the neutron irradiations performed by Weck *et al.*[3] The five-parameter fits obtained for the present results were generally much satisfactory. However, for the most-highly-doped Bi-Sn sample studied at 4 K (Bi-Sn VI), the fit suddenly became impossible for the 2.5-MeV irradiation and for more than 1.5×10^{-4} dpa, for an unknown reason.

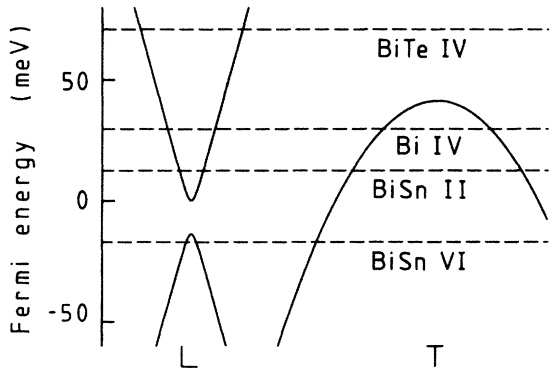

FIG. 1. Schematic band structure of bismuth in the vicinity of the Fermi level. At L points, for pure bismuth (sample Bi IV), three equivalent pseudoellipsoids of electrons are present, and at T points one ellipsoid of holes is present. The Fermi levels for the three other samples used in 4-K experiments are also represented.

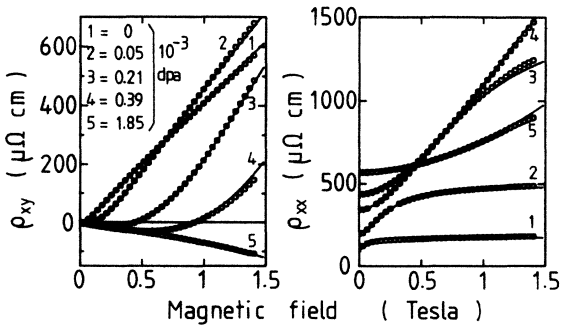

FIG. 2. Hall resistivity (left) and magnetoresistivity (right) vs magnetic field taken at 4 K for a few doses for the Bi-Sn II sample. The discrete points are the experimental values and the solid lines correspond to our fits as described in Sec. II C.

III. THE 4-K EXPERIMENTS

A. Results

Figures 3 and 4 give the "production curves," i.e., the resistivity versus electron dose for the 4-K samples irradiated at 2.5 MeV. Except in the case of the Bi-Te sample, one can see that the curves are very nonlinear, even at low dose. In contrast with metals, the resistivity increments are very important and quickly exceed the initial value of resistivity.

In Figs. 5–7 we display the results of the analysis of the same 2.5-MeV irradiation when galvanomagnetic data are taken into account. We recall that the analysis for Bi-Sn VI became impossible for doses superior to 1.5×10^{-4} dpa; even for lower doses the fit is not very reliable (μ_x, which for this sample is relative not to electrons but to light holes, is found to increase versus dose; however, the carrier-concentration values are believed to make sense). Figure 5 gives $N-P$ versus dose: all the curves display a negative curvature; the two Bi-Sn samples show much higher initial slopes than the Bi and Bi-Te ones. Figures 6 and 7 give variations of the inverse of the mobilities during irradiation: these curves are always increasing, as in metals; however, they are not always linear and show a more or less pronounced saturation. Table II gives a summary of the results at low dose, i.e., initial values and slopes for N-P and the mobilities. The table includes the 2.5- and 1-MeV results; for this last energy only low-dose measurements were made.

B. Discussion

In Ref. 9 we wrote the equation of electrical neutrality,

$$N-P=[\mathrm{Te}]+\alpha c\ , \tag{1}$$

which applies to dilute Bi-Te alloys: N and P are, respectively, the electrons and hole concentrations, [Te] the tellurium content, c the defect concentration, and α the mean charge per defect. We always follow Noothoven van Goor's assertion[10] that tellurium and tin are, respec-

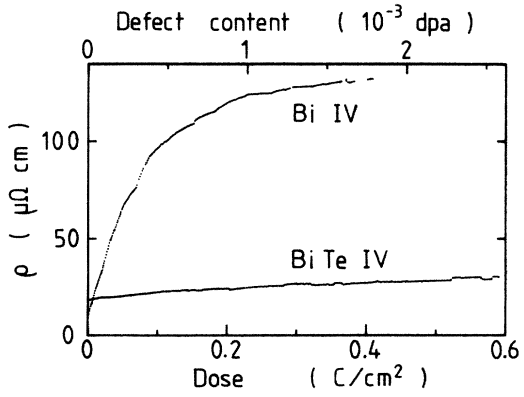

FIG. 3. Production curves (i.e., resistivity vs electronic dose) for the Bi IV and Bi-Te IV samples irradiated at 2.5 MeV in the 4-K experiment. A scale giving the defect concentration is added. The experimental errors on the resistivity values are thought to be of the order of the point dispersion.

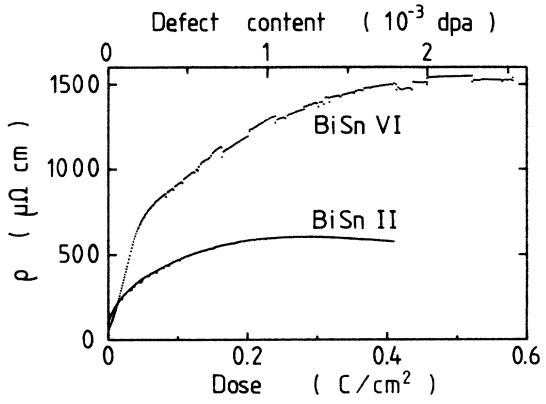

FIG. 4. Production curves for the Bi-Sn II and Bi-Sn VI samples under the same conditions as Fig. 3.

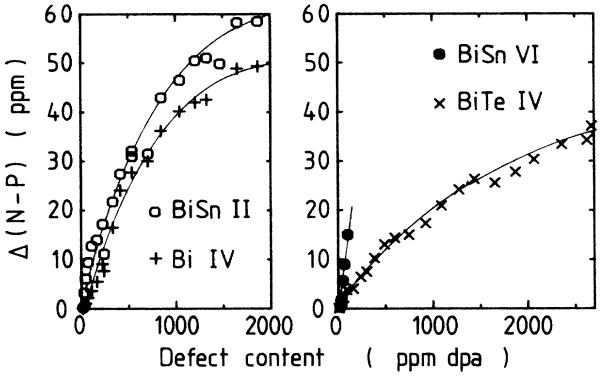

FIG. 5. Relative number of carriers vs defect concentration for the four samples of the 4-K experiment. The solid lines are guides for the eye. For the Bi-Sn VI sample the analysis of the magnetotransport data became impossible quickly. It is hard to evaluate the errors made on such quantities coming from a fit; however, the continuity of the curves is considered very encouraging.

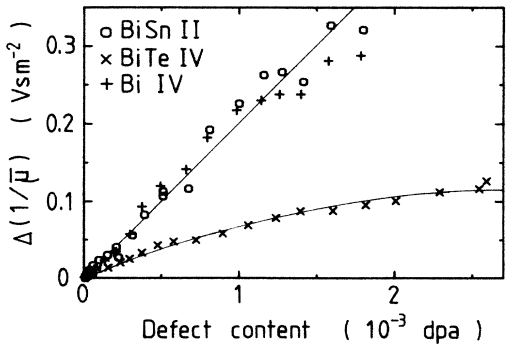

FIG. 6. Inverse of the electron mobility $\bar{\mu}$ (with the zero-dose contribution subtracted) vs defect concentration for the Bi IV, Bi-Sn II, and Bi-Te IV samples irradiated at 2.5 MeV in the 4-K experiment. The lines are guides for the eye.

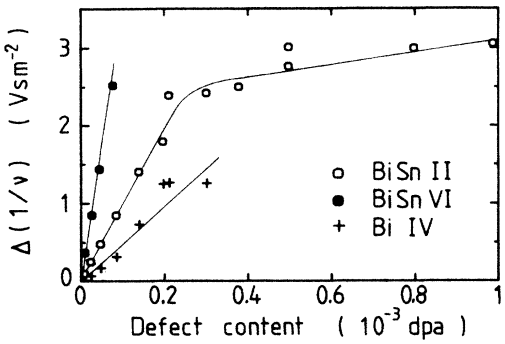

FIG. 7. Inverse of the hole mobility ν (with the zero-dose contribution subtracted) vs defect concentration for the Bi IV, Bi-Sn II, and Bi-Sn VI samples irradiated at 2.5 MeV in the 4-K experiment. In the Bi-Te IV sample, no holes are present. The lines are guides for the eye.

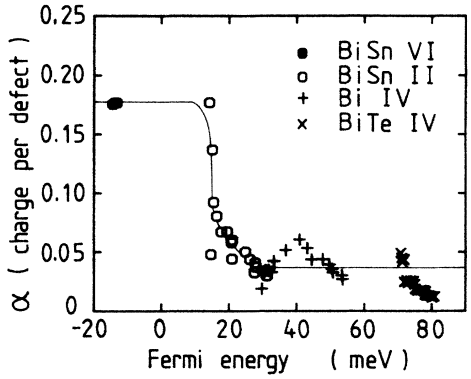

FIG. 8. Mean charge per irradiation defect vs Fermi energy for the four samples of the 4-K experiment. The solid line is a guide for the eye.

tively, a monovalent donor and acceptor in bismuth. In the case of tin-based alloys, it is clear that the electrical neutrality can be written as

$$N-P-P_l=\alpha c-[\mathrm{Sn}]\ , \tag{2}$$

where P_l is the concentration of the eventual light holes. In Ref. 9 an indirect determination of the α value versus electron energy was possible in the case of a Bi-Te sample. The determination is much more direct here: N, P P_l, [Te], or [Sn] are known by Hall-effect measurements and c by dose determination associated with the knowledge of the cross sections, so that α is known as a function of c. On the other hand, the Lax model enables us to compute without ambiguity the Fermi-energy value E_F when the carrier concentrations are known. We thus present Fig. 8, where α versus E_F is plotted in the case of the 2.5-MeV experiment. The salient features of Fig. 8 are (i) the data coming from each sample fit together on a more or less unique curve, and (ii) the presence of a strong decrease of the α value for $E_F \simeq 18$ meV between two plateaus at 0.18 and 0.04, respectively. The data from the 1-MeV experiment consist of only one point per sample in the α/E_F plot. The results are more scattered (see Table II) than at 2.5 MeV; however, they seem to be consequent with an α value independent of E_F and roughly equal to the low E_F value at 2.5 MeV: $\alpha \simeq 0.18$.

At this stage we propose a model for the behavior of α consistent with Ref. 9. We attribute to the Frenkel pair—the only defect created at 1 MeV irradiation—a constant (i.e., Fermi-level-independent) α value equal to 0.18. At 2.5 MeV, besides the Frenkel pairs, more complicated defects are created, which we shall term "complexes." These complexes are thought to be responsible for the sharp decrease of α in Fig. 8. We believe that there exists, at $E_F \simeq 18$ meV, a virtual bound state attributed to complexes whose width is about 5 meV. This state is associated with an acceptor level which is nonionized when E_F is below it and ionized when above it. Such a model is coherent with the conclusions of our displacement-threshold-energy measurements,[9] from which we deduced the donor character of the Frenkel pair and the acceptor character of complexes. It is worth noting that the fits corresponding to the 18-meV region are generally less good than elsewhere, a fact which is perhaps related to the existence of the virtual bound state. Finally, we can mention here some experimental evidence that we noticed during 2.5-MeV irradiations: the two Bi-Sn samples, and only these two, display persistent photoconductivity; this happens when the Fermi level is in the region around 18 meV. We discovered this fact the following way: In order to get a stable temperature for the resistivity measurements, we interpose from time between the electron beam and the samples a copper target which stops the beam but produces some x rays with a broad energy spectrum. Under this x-ray irradiation the resistivity exhibited a slow, nonexponential decrease, with a typical characteristic time of 500 s. A relaxation in the opposite direction occurred when the electron beam was stopped. No such photoconductivity was observed in the Bi or Bi-Te samples, or in the Bi-Sn samples whose Fermi level was well below 18 meV, that is, at

TABLE II. Initial values of the parameters in the 4-K experiment.

Sample	$N-P$ (ppm)	$\alpha=$ $d(N-P)/d(\sigma\varphi)$ 1 MeV	2.5 MeV	$1/\bar{\mu}$ (10^{-3} V s m^{-2})	$d(1/\bar{\mu})/d(\sigma\varphi)$ (10^{-5} V s m^{-2}/ppm) 1 MeV	2.5 MeV	$1/\nu$ (V s m^{-2})	$d(1/\nu)/d(\sigma\varphi)$ (10^{-3} V s m^{-2}/ppm) 1 MeV	2.5 MeV
Bi IV	−0.02	0.11	0.04	4.04	17.3	16.5	0.029	5.8	4.5
Bi-Te IV	104.7	0.23	0.06	86.7	33.0	11.6	no holes		
Bi-Sn II	−53.8	0.17	0.18	16.5	18.7	19.3	0.406	8.8	10
Bi-Sn VI	−212.6	0.31	0.18	32.2	83.11	?	0.775	10.2	31

TABLE III. Mobility-parameter values for electron and holes.

$\bar{\mu}_0$ (m^2/V s)	ν_0 (m^2/V s)	s_d (V s m)	t_d (V s m)	s_{Sn} (V s m)	s_{Te} (V s m)	t_{Sn} (V s m)
250	34	7×10^{-27}	2.1×10^{-25}	2×10^{-26}	2×10^{-26}	1.75×10^{-25}

the beginning of the irradiation. These facts are coherent with the existence of a virtual bound state in the 18-meV region.

In Ref. 9 we could deduce a value for the so-called s_d parameter, which is the differential of the inverse electronic mobility with respect to the concentration of defects, from the equation

$$1/\bar{\mu}=1/\bar{\mu}_0+cs_d \ , \tag{3}$$

where $\bar{\mu}$ is the electron mobility in the x-y plane averaged on the three electron ellipsoids, $\bar{\mu}_0$ being the mobility for zero dose. The present 4-K experiments give us (see Table II) a direct determination of the s_d value from the dose dependence of the inverse of the mobility $\bar{\mu}$. In a similar way we get a value for t_d, the corresponding parameter for holes. All the following values are taken at low dose.

From the 1-MeV experiments we get

$$s_d=(6.2-12.0)\times10^{-27} \text{ V s m} \ ,$$

$$t_d=(2.0-3.1)\times10^{-25} \text{ V s m} \ ,$$

whereas 2.5-MeV experiments give

$$s_d=(4.2-6.9)\times10^{-27} \text{ V s m} \ ,$$

$$t_d=(1.6-3.5)\times10^{-25} \text{ V s m} \ .$$

The s_d values are in good agreement with the value of 7×10^{-27} V s m given in Ref. 9. In fact in the case of a dilute alloy, one more term must be added in the mobility equation above, which can be written as

$$1/\bar{\mu}=1/\bar{\mu}_0+[\text{Sn}]s_{\text{Sn}}+cs_d \ , \tag{4}$$

where the s_{Sn} parameter is the differential of the inverse electronic mobility with respect to tin concentration. The equivalent equation for holes involves the coefficients t_d and t_{Sn}:

$$1/\nu=1/\nu_0+[\text{Sn}]t_{\text{Sn}}+ct_d \ . \tag{5}$$

In the case of Bi-Te alloys one introduces the s_{Te} coefficient. Our 4-K experiments enable us to give, with a quite high uncertainty, the order of magnitude of all these mobility coefficients. These are summarized in Table III; one can notice that they are in rough agreement with the values established by Noothoven van Goor.[10]

IV. 20-K EXPERIMENTS

A. Results

Figures 9 and 10 give the production curves for several Bi-Te, Bi, and Bi-Sn samples. These samples constitute only a part of the samples actually irradiated and were chosen so as to be representative of the different kinds of behavior. The main characteristics of the curves we obtained are the following.

(i) For Bi-Te samples the production curve is quite linear, corresponding to relatively small resistivity increments. At high dose a negative curvature becomes apparent.

(ii) For the pure Bi sample the slope is quite high for the lowest doses, decreases strongly, reaches an inflexion point, and becomes more or less constant at higher doses. In this high-dose regime the behavior and the slope of the pure Bi production curve is comparable to that of the Bi-Te samples. The whole production curve is invariant when a sample with its z axis along the current direction and its x axis perpendicular to the sample is taken (sample Bi I, see Fig. 9).

(iii) The behavior of the Bi-Sn samples is the most complicated, although it follows qualitatively that of the pure Bi samples: very high slopes for low doses, and much lower ones at higher fluences with a more or less linear regime. As the Sn concentration increases, a maximum appears at medium fluences, followed by a minimum (not always reached in the case of the highest Sn contents). Both the dose and the resistivity values for which the maximum appears increase strongly with increasing Sn concentrations. For Sn concentrations higher than about 150 ppm, the curvature of the production curve is positive at the beginning of the irradiation. At higher dose an inflexion point occurs, followed by a point where there is quite a rapid, quasidiscontinuous decrease of the slope: this is also apparent in the 4-K experiment in the case of the 213-ppm sample (Bi-Sn VI), see Fig. 4.

(iv) A few resistivity production curves were obtained

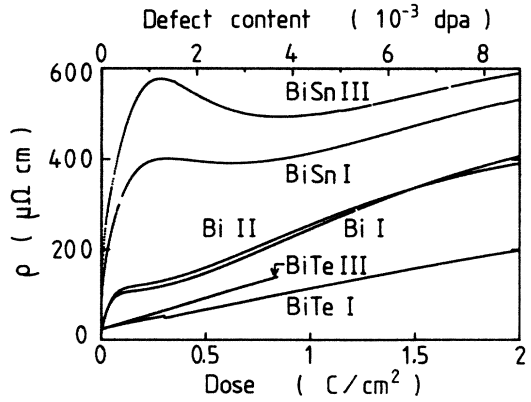

FIG. 9. Production curves (i.e., resistivity vs electronic dose) for six samples irradiated at 2.5 MeV in the 20-K experiment. A scale giving the defect concentration is added. Note the noiseless character of the curves.

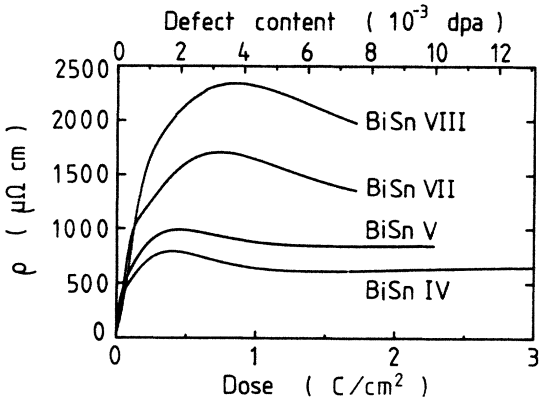

FIG. 10. Production curves for four Bi-Sn samples irradiated at 2.5 MeV in the 20-K experiment.

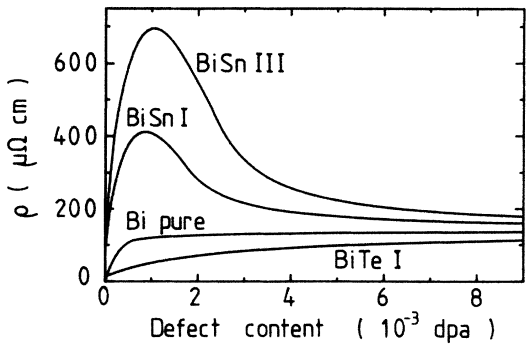

FIG. 11. Simulation of the production curves of Fig. 9 based on the simple model discussed in Sec. IV B.

for pure Bi and some alloys for irradiating energies of 1 and 1.5 MeV. The curves obtained show the same qualitative behavior as at 2.5 MeV. However, the characteristic points of the curve, particularly the maximum, always happen at lower defect concentrations and for often much lower resistivity values. The curves for different energies differ mainly at high dose; in particular, for low dose the resistivity–versus–defect-concentration law is seen to be independent of energy for pure Bi (see Ref. 9).

B. Model

We make use here of the data collected from the analysis of the 4-K experiments; we take into account (in the case of doping with tin) Eqs. (4) and (5). The numerical data collected in Table III are considered. Equations (4) and (5) are to be understood as Matthiessen's rule, i.e., additivity of the different scattering probabilities for each kind of carrier: we exclude all resonant contribution of the virtual bound state to the scattering, a fact commented on in the discussion below.

The electrical conductivity is written as

$$\sigma = Ne\bar{\mu} + Pev \ , \tag{6}$$

where the values for the carrier concentrations are given by (i) the Lax model,[12] which gives a relation between N and P, and (ii) the electrical neutrality equation, which is given, in the case of doping with tin, by Eq. (2). The results of Sec. III B give sufficient knowledge of the behavior of α versus Fermi energy. Here we model this behavior by the equation

$$\alpha = \alpha_{\min} + (\alpha_{\max} - \alpha_{\min})\{\tfrac{1}{2} - \pi^{-1}\arctan[(E_F - E_d)/\Delta]\} \ , \tag{7}$$

where $E_d = 18$ meV, $\Delta = 5$ meV, $\alpha_{\max} = 0.18$, and $\alpha_{\min} = 0.03$. The arctangent function corresponds to the Lorentzian density of states found for the virtual bound state in the Anderson model[15] in the case of a nearly constant density of state in the conduction band; this must be considered here as a rough first approximation.

Figures 11 and 12 give the production curves simulated by this model, obtained for tin or tellurium concentrations equal to those of the samples whose experimental data were given in Figs. 9 and 10.

C. Discussion

From the comparison of the experimental and simulated curves, some features are in quite good agreement and some others are not.

The general agreement between the experiment and the model is rather satisfactory: The model predicts the existence of a maximum in the production curve of Bi-Sn samples and its nonexistence for pure Bi and Bi-Te samples. It accounts qualitatively for the shape of the Bi-Sn curves at low dose, i.e., for the variation of the curvature with dose. It also predicts quasilinearity in the case of Bi-Te. Concerning the initial slopes, we give in Table IV their values, both measured and predicted by the present model; the fit is rather good. The general fact that the curves obtained at 1 MeV always lie below the curves obtained at 2.5 MeV is also taken into account by our model if, in the 1-MeV case, a constant value for α ($\alpha = \alpha_{\max}$) is introduced.

However, there are some important discrepancies. The absolute value of the resistivity for a given dose becomes much too high for tin concentrations higher than 100

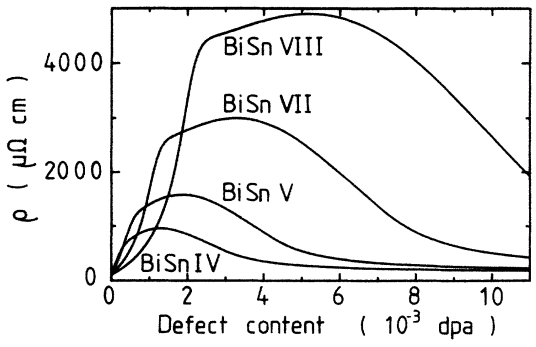

FIG. 12. Simulation of the production curves of Fig. 10 based on the simple model exposed in Sec. IV B.

TABLE IV. Initial values of the slope of the resistivity production curves during 2.5-MeV irradiation at 20 K.

Sample	Initial slope ($\mu\Omega$ cm/% of dpa) Expt.	Calc.
Bi I	6940	3570
Bi II	8090	3570
Bi III	4390	3570
Bi IV	4330	3570
Bi-Te I	289	536
Bi-Te II	578	509
Bi-Te III	364	415
Bi-Te IV	174	369
Bi-Sn I	12 700	11 700
Bi-Sn II	22 600	14 800
Bi-Sn III	20 800	17 400
Bi-Sn IV	24 300	17 600
Bi-Sn V	27 700	12 200
Bi-Sn VI	23 000	7680
Bi-Sn VII	13 900	6460
Bi-Sn VIII	8100	3670

ppm. It is possible that this fact has something to do with our inability to analyze the magnetotransport data at 4 K for the Bi-Sn VI sample. Moreover, one can note a general discrepancy at higher doses for all the samples. This last point is examined in the next subsection.

We tried[1] to include in our model some resonant contribution of the virtual bound state to the carriers scattering and in every case we found very bad agreement, the conclusion being that if any resonant coupling exists it can only be between the localized state and the holes (which play a minor role in the conductivity in this range of E_F) and cannot involve electrons.

D. High-dose saturation

The experimental data of Figs. 9 and 10 display, except for the most-highly-doped Bi-Sn samples ([Sn] $\geq$ 100 ppm), a quasilinear variation of resistivity versus dose for doses corresponding to more than 6×10^{-3} dpa, with a tendency to saturate (negative curvature). Such a behavior recalls that of a good metal, which is consistent with the fact found in Sec. III B that the Fermi level is nearly blocked at high defect concentrations: α becomes small when E_F is above E_d, the defect-level energy. We shall treat the high-dose regime of the samples Bi-Te, Bi, and Bi-Sn with Sn content less than 100 ppm in the scope of the recombination-volume model.[16] One states that a defect, created in a volume v_0 surrounding an already existing defect, annihilates itself, so that the probability of creating one defect under certain irradiation conditions is reduced by a term containing the defect concentration c. One can write

$$\frac{dc}{d\varphi}=\sigma(1-v_0c)\ , \tag{8}$$

where c is the defect concentration (in dpa), φ the electron dose, σ the displacement cross section, and v_0 the recombination volume expressed in a dimensionless unit (number of atomic volumes). If at high dose the resistivity increment $\Delta\rho$, taken from an arbitrary origin, is proportional to c,

$$\Delta\rho=Ac\ , \tag{9}$$

we can write its derivative $\Delta\dot{\rho}$ versus φ as

$$\Delta\dot{\rho}=A\frac{dc}{d\varphi}=A\sigma-\sigma v_0\varphi\ , \tag{10}$$

which means that the plot of $\Delta\dot{\rho}$ versus $\Delta\rho$ must be a straight line whose slope will give directly v_0. In Fig. 13 we give the curves obtained for three typical samples. For the highest doses (large $\Delta\rho$ values) the curves become linear with slopes quite identical for all samples. In Table V we sum up the results; v_0 was computed with a value of 700 b taken for σ at 2.5 MeV. The values for v_0 range from 98 to 190 atomic volumes, and are slightly higher in pure bismuth samples than in dilute alloys.

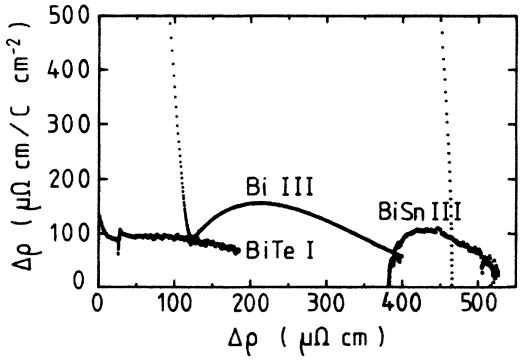

FIG. 13. Derivative of the resistivity with dose vs the resistivity increment for three samples irradiated at 2.5 MeV in the 20-K experiment. The curves become nearly linear with a negative slope in the high-dose (high-$\Delta\rho$) regime.

TABLE V. Recombination volumes in the 20-K experiment.

Sample	$\Delta\dot{\rho}/\Delta\rho$ (cm^2/C)	v_0 (atomic volumes)
Bi I	0.68	158
Bi II	0.82	190
Bi III	0.65	151
Bi-Te I	0.43	98
Bi-Te II	0.51	117
Bi-Te III	0.49	112
Bi-Sn III	0.54	126

V. CONCLUSIONS

The whole set of resistivity and magnetotransport measurements described in the present paper enabled us to confirm and extend the conclusions of Ref. 9. The irradiation defects are globally donors; however, their effect depends remarkably on the electron irradiation energy, i.e.,

on the precise nature of the defects. One can classify very roughly the defects into two classes: simple ones (Frenkel pairs, which are created alone at energies lower than 1.2 MeV) and more complicated ones (small point-defect complexes, which appear roughly at an energy corresponding to twice the threshold energy, so that one may think that they are principally divacancies). We attribute two distinct electrical behaviors to the two classes. The "simple" defects are donors, always with the same charge around 0.18 per defect. The "more complicated" ones seem to be associated with a virtual bound state, situated in the band overlap ($E_F = 18$ meV, width $\Delta = 5$ meV): these defects are nonionized (neutral) when the Fermi level is below this defect level and are ionized (acceptors) above it. The present measurements are unable to specify whether the vacancy or the interstitial, or both, are electrically active. However, in Ref. 9 we reinterpreted the quenching experiments of Bittar and Lesueur,[4] showing that the vacancy is a donor in bismuth. As a consequence, we deduced that the interstitial is not far from being neutral. Moreover, our annealing experiments, which are to be published in the near future, support the donor character of the vacancy.

ACKNOWLEDGMENTS

Numerous discussions with D. Lesueur are gratefully acknowledged.

[1]P. Bois, Ph.D. thesis, Université d'Orsay, 1986 (unpublished); Commissariat à l'Energie Atomique Report No. CEA-R-5389, 1987 (unpublished).

[2]B. Legros–de Mauduit and F. Reynaud, Cryst. Lattice Defects **9**, 141 (1982).

[3]W. Weck, H. Gerstenberg, and P. Müller, in *Proceedings of the 17th International Conference on Low-Temperature Physics–LT-17, Karlsruhe, 1984,* edited by U. Eckern, A. Schmid, W. Weber, and H. Wühl (North-Holland, Amsterdam, 1984), p. 1383.

[4]A. Bittar and D. Lesueur, Phys. Status Solidi A **48**, K123 (1978).

[5]G. Quélard and D. Lesueur, Phys. Status Solidi A **36**, 729 (1976).

[6]G. Quélard, J. Dural, J. Ardonceau, and D. Lesueur, Radiat. Effects **39**, 45 (1978).

[7]M. Le Goff and J. Heremans, J. Phys. F **14**, 399 (1984).

[8]C. Corbel, P. Bois, P. Moser, and I. Lemahieu, in Proceedings of the Xth International Conference on Vacancies and Interstitials in Metals and Alloys, Berlin, 1986 [Mater. Sci. Forum **15-18**, 721 (1987)].

[9]P. Bois and F. Beuneu, J. Phys. F **17**, 2365 (1987).

[10]J. M. Noothoven van Goor, Philips Res. Rep. Suppl. **4** (1971).

[11]V. S. Edel'man, Adv. Phys. **25**, 555 (1976).

[12]B. Lax, Rev. Mod. Phys. **30**, 122 (1958).

[13]B. Abelès and S. Meiboom, Phys. Rev. **101**, 544 (1956).

[14]R. Fletcher and M. J. D. Powell, Comput. J. **6**, 163 (1963).

[15]P. W. Anderson, Phys. Rev. **124**, 41 (1961).

[16]H. J. Wollenberger, *Vacancies and Interstitials in Metals* (North-Holland, Amsterdam, 1969).